THE JOURNAL OF PHYSICAL CHEMISTRY B

Article

pubs.acs.org/JPCB

Revised Parameters for the AMOEBA Polarizable Atomic Multipole Water Model

Marie L. Laury,[†,∥] Lee-Ping Wang,[‡,∥] Vijay S. Pande,[‡] Teresa Head-Gordon,[§] and Jay W. Ponder*[,†]

[†]Department of Chemistry, Washington University in St. Louis, St. Louis, Missouri 63130, United States

[‡]Department of Chemistry, Stanford University, Stanford, California 94305, United States

[§]Department of Chemistry, University of California, Berkeley, California 94720, United States

Supporting Information

ABSTRACT: A set of improved parameters for the AMOEBA polarizable atomic multipole water model is developed. An automated procedure, ForceBalance, is used to adjust model parameters to enforce agreement with *ab initio*-derived results for water clusters and experimental data for a variety of liquid phase properties across a broad temperature range. The values reported here for the new AMOEBA14 water model represent a substantial improvement over the previous AMOEBA03 model. The AMOEBA14 model accurately predicts the temperature of maximum density and qualitatively matches the experimental density curve across temperatures from 249 to 373 K. Excellent agreement is observed for the AMOEBA14 model in comparison to experimental properties as a function of temperature, including the second virial coefficient, enthalpy of vaporization, isothermal compressibility, thermal expansion coefficient, and dielectric constant. The viscosity, self-diffusion constant, and surface tension are also well reproduced. In comparison to high-level *ab initio* results for clusters of 2−20 water molecules, the AMOEBA14 model yields results similar to AMOEBA03 and the direct polarization iAMOEBA models. With advances in computing power, calibration data, and optimization techniques, we recommend the use of the AMOEBA14 water model for future studies employing a polarizable water model.

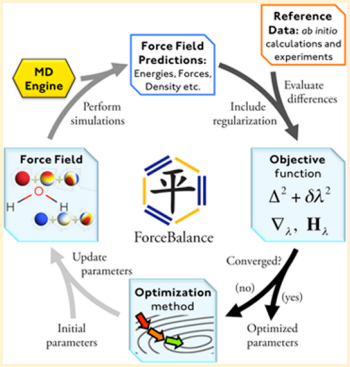

INTRODUCTION

"What does a fish know about the water in which he swims all his life?" ~Albert Einstein ("Self Portrait", 1936)
"Water is the most extraordinary substance! Practically all its properties are anomalous..." ~Albert Szent-Georgi ("The Living State", 1972)

Empirical models of water play an important role in the prediction and rationalization of bulk water properties. One of the first water models was proposed by Bernal and Fowler in 1933.[1] Before the advent of digital computers, this simple atomistic model was used to deduce the crystal structure of ice, the X-ray diffraction curve for water, and the heat of solution of ions. Water was among the first molecular systems to be simulated at the atomic level via Monte Carlo[2] and molecular dynamics (MD) techniques.[3] The ST2 water model, used throughout much of the early computational work, showed simple distributed point charge models could be tailored to reproduce bulk properties.[4] Elaboration of fixed point charge models led to the development of the widely used TIP3P,[2] TIP4P,[2] and SPC[5] potentials, as well as the subsequent ST4,[6] TIP5P,[7] SPC/E,[8] TIP4P-Ew,[9] and F3C[10] potentials, among many others. All of these water models have been used as the foundation for development of various biomolecular force fields; therefore, many of the models are still commonly used for explicit solvent calculations on biological systems.

A tremendous variety of specialized water potentials have been proposed for accurate modeling of molecular cluster data and selected bulk properties. These specialized potentials are typically parametrized and calibrated against accurate and reliable *ab initio* results for small numbers of molecules and include an explicit accounting of electronic polarization. Perhaps the first pair-interaction water model to be systematically constructed from *ab initio* data was the original MCY model from 1976.[11] Early attempts at polarizable models include Vesely's work with Stockmayer potentials[12] and the polarizable electropole model of Barnes et al.[13] Kuwajima and Warshel later incorporated explicit polarization into a modified potential inspired by the MCY work.[14] Other early polarizable potentials were provided by Sprik and Klein,[15] the NEMO method,[16] the POL3 model from Kollman's group,[17] and Dykstra's MMC model.[18] While a complete list is far too long to present here, more recent members extending this class would include TTM3-F,[19] SWM4-DP,[20] DPP2,[21] etc. Key features of such water models include the ability to reproduce with high fidelity the electrostatic potential around an isolated water molecule, and the ability of individual molecules to respond to their local environment. Some water potentials, such as TTM3, couple

Special Issue: Branka M. Ladanyi Festschrift

Received: October 30, 2014
Revised: February 15, 2015
Published: February 16, 2015

DOI: 10.1021/jp510896n
J. Phys. Chem. B 2015, 119, 9423−9437

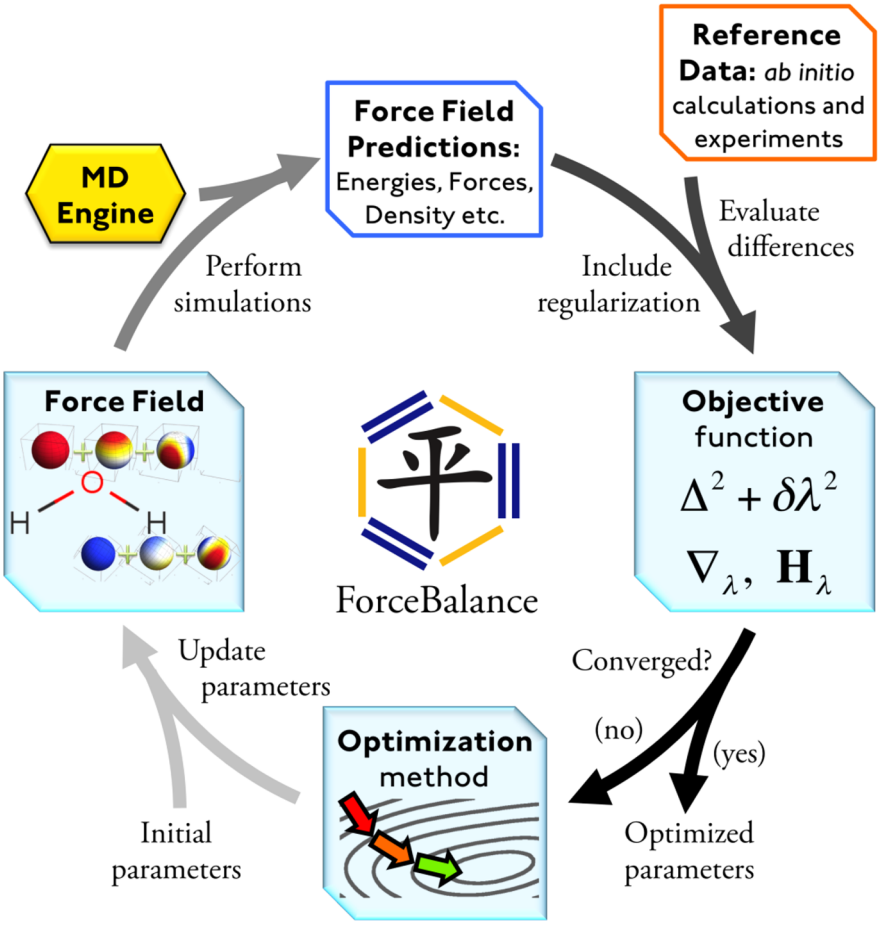

Figure 1. ForceBalance procedure. Calculation begins with an initial set of parameters (lower left), which is used to generate a force field and perform simulations (upper left). The objective function is a weighted sum of squared differences between the simulation results and the reference data (right), plus a regularization term used to prevent overfitting. The optimization method (bottom) updates the parameters in order to minimize the objective function.

the electrostatic representation to the structure of the molecule as specified by valence terms.

Much of chemistry can be rationalized at the level of partial charge interactions based on electronegativity arguments and inductive effects. To yield an accurate representation of an electrostatic potential usually requires a molecular description beyond simple partial atomic charges.[22] While atom-centered charge fitting schemes such as RESP[23] are extensively employed to parametrize force fields, the typical result is a relative error of several percent over an envelope close to, but outside of, the van der Waals surface of a polar molecule. One solution to improve upon the partial atomic charge water models is to include polarizability, as in the atomic multipole optimized energetics for biomolecular applications (AMOEBA) force field. The advantages of a polarizable model are evident in heterogeneous systems, for example, water−ion mixtures. Both cations and anions are highly polarizing, and the larger anions in particular are also very polarizable. While it is certainly possible for nonpolarizable force fields to provide reasonable bulk phase structural and thermodynamic properties,[24] a fully polarizable model should have an advantage in terms of transferability. Ion parameters derived against gas phase ion−water *ab initio* calculations adapt seamlessly to condensed phase modeling.[25]

While the AMOEBA model goes beyond typical fixed-charge empirical potentials via inclusion of higher order permanent multipoles and dipole polarizability, it neglects quantum nuclear effects (QNEs) such as zero-point energy. In keeping with the traditional formulation of molecular mechanics force fields, AMOEBA is an attempt to reproduce the Born−Oppenheimer potential energy surface (BO-PES) in terms of simple classical potential functions. As such, AMOEBA results can be directly compared to and parametrized against a corresponding BO-PES derived from *ab initio* electronic structure calculations. The issues surrounding QNE arise when AMOEBA is used to model dynamic properties at finite temperature, as in MD simulations aimed at modeling properties of water in the bulk phase. One approach is to explicitly include QNE in the calculations by performing path integral molecular dynamics (PIMD),[26] or a recent variant such as ring-polymer (RPMD) simulations.[27] Several path-integral-based studies of liquid water structure and properties have been reported over the past three decades.[28−36] As has been noted,[26] these simulations do not reproduce the dynamics of the real quantum system but provide an isomorphic system in which QNE-corrected properties can be evaluated.

Provided the QNE are reasonably small for properties and temperatures of interest, a second possibility is to implicitly account for such effects in the model parametrization while evaluating properties via classical MD methods. This approach is perhaps best viewed as a parameter renormalization to account for the approximate nature of the classical simulations.[32] For properties where the quantum corrections are larger, estimates of the correction are often well-known and can be added to the

DOI: 10.1021/jp510896n
J. Phys. Chem. B 2015, 119, 9423−9437

classical result prior to comparison with experiment.[37] As will be discussed below, we have chosen to implicitly include quantum nuclear effects in AMOEBA. Retaining the use of classical simulation technology for use with AMOEBA has two advantages: (1) increased computational efficiency and ease of parametrization and (2) compatibility with existing AMOEBA parameters developed for a variety of systems including ions, small organic molecules, transition metal complexes, proteins, and nucleic acids.

The choice of water potential is often a key first step in construction of a general-purpose molecular force field. Water is a ubiquitous solvent, and the balance of solvent−solvent, solvent−solute, and solute−solute interactions often plays a critical role in determining solute behavior. Computation of relative hydration free energies and ligand binding energies is aided by cancellation of errors in force field models. However, accurate calculation of absolute free energies generally requires a fine balance between solvent and solute interactions. Errors in the solvent−solvent potential will systematically recur in all subsequent calculations involving solvent. This explains the fact that the most current biomolecular force fields are explicitly or implicitly parametrized for use with a particular water model. For example, recent revision of the Amber nonpolarizable force field for use with the TIP4P-Ew water model involved a substantial reworking of the protein parameter values[38] or the elimination of the simple mixing rules to combine these force fields by explicitly parametrizing for the solute−solvent interactions themselves.[39]

Fitting of model parameters can be carried out manually via a trial and error method, or an automated procedure can be employed. Least squares optimization of force fields first began with the consistent force field proposed by Lifson and Warshel in the 1960s.[40] Other early efforts extended least-squares optimization through use of *ab initio* calculations[41] and application to bulk phase crystal modeling.[42] Recently, force matching techniques have played a major role in development of both atomistic and coarse grained models.[43−45] ForceBalance[46−48] (Figure 1) extends this prior work in several directions, including the ability to use a larger and more diverse data set which includes experimental liquid phase measurements and *ab initio* calculations. The overall objective function is expressed as a weighted sum of squared residuals over the experimental and theoretical target data sets. Recently, ForceBalance has been used to derive two new, rigid, fixed partial charge water models, TIP3P-FB and TIP4P-FB.[48]

In the present work, we derive a revised set of parameters for the AMOEBA water model using the ForceBalance methodology. The new model, to be referred to as AMOEBA14, represents a significant improvement over the original 2003 AMOEBA water parametrization[49] (herein referred to as AMOEBA03). The AMOEBA14 model provides a significant improvement in the ability to predict experimental and *ab initio* data, particularly for a number of liquid properties across a range of temperatures. In addition, we provide some initial results to show the new model is capable of yielding acceptable results of ion−water energetics, which holds promise of compatibility of AMOEBA14 water with the previously determined AMOEBA force fields for organic molecules[50] and for proteins.[51]

METHODOLOGY

AMOEBA Model. The atomic multipole optimized energetics for biomolecular applications (AMOEBA)[49] water model in this work has the functional form

$$E = E_{\text{bond}} + E_{\text{angle}} + E_{\text{b}\theta} + E_{\text{vdW}} + E_{\text{ele}}^{\text{perm}} + E_{\text{ele}}^{\text{ind}} \quad (1)$$

The first three terms describe the short-range interactions, including bond stretching, angle bending, and the Urey−Bradley bond-angle cross term. The bond stretching parameters include anharmonicity up to second order deviations from the ideal bond length

$$E_{\text{bond}} = K_{\text{b}}(b - b_0)^2[1 - 2.55(b - b_0) - 3.793125(b - b_0)^2] \quad (2)$$

and the angle bending function includes up to fourth order deviations from the ideal angle

$$E_{\text{angle}} = K_\theta(\theta - \theta_0)^2[1 - 0.014(\theta - \theta_0) + (5.6 \times 10^{-5})(\theta - \theta_0)^2 - (7.0 \times 10^{-7})(\theta - \theta_0)^3 + (2.2 \times 10^{-8})(\theta - \theta_0)^4] \quad (3)$$

The Urey−Bradley parameters follow a harmonic functional form

$$U_{\text{UB}} = K_l(l - l_0)^2 \quad (4)$$

The remaining three terms in eq 1 describe the nonbonded van der Waals (vdW) interactions and the electrostatic contributions from both permanent and induced dipoles. The vdW term follows a Halgren buffered 14-7 potential to model the pairwise additive interactions for dispersion at long-range and exchange repulsion at short-range[52]

$$E_{ij}^{\text{buff}} = \varepsilon_{ij}\left(\frac{1+\delta}{\rho_{ij}+\delta}\right)^{n-m}\left(\frac{1+\gamma}{\rho_{ij}^m+\gamma} - 2\right) \quad (5)$$

and which is less steep than the Lennard-Jones functional form. The nonbonded van der Waals (vdW) parameters we use are $n = 14$, $m = 7$, $\delta = 0.07$, $\gamma = 0.12$, the well depth ε_{ij}, and $\rho_{ij} = (R_{ij}/R_{ij}^0)$, where R_{ij} is the i−j separation and R_{ij}^0 is the minimum energy distance. van der Waals parameters are included for both oxygen and hydrogen atoms. The hydrogen reduction factor moves the hydrogen vdW center toward the oxygen along the bond length. For example, a reduction factor of 0.80 would move the hydrogen vdW center 20% of the bond length toward the oxygen.

The permanent electrostatic term includes the atomic monopole, dipole, and quadrupole moments for each atom center. The polarization effects within the AMOEBA water model include mutual polarization by mutual induction of the dipoles for each atom. The nonadditive definition of the model translates to each atom within the water molecule being a polarizable site and experiencing the mutual polarization. As a consequence of the nonadditive mutual definition of the AMOEBA model, a polarization catastrophe would arise if a damping scheme were not introduced; therefore, the polarization parameters for the AMOEBA water model include the polarizability of oxygen and hydrogen and a damping factor related to Thole's description of damping.[53] The distribution of the charge (ρ) in AMOEBA has the functional form

$$\rho = \frac{3\alpha}{4\pi}\exp(-au^3) \quad (6)$$

where a represents the damping parameter[53] controlling how strongly the charge distribution is smeared and u is the distance relating the polarizabilities of atomic sites i and j [$u = R_{ij}/(\alpha_i\alpha_j)^{1/6}$].

DOI: 10.1021/jp510896n
J. Phys. Chem. B 2015, 119, 9423−9437

For the mutual model, the induced dipole is calculated at each atomic site via

$$\mu_{i,\alpha}^{\text{induc}} = \alpha_i E_{i,\alpha} = \alpha_i\left(\sum_{\{j\}} T_\alpha^{ij} M_j + \sum_{\{j\}} T_{\alpha\beta}^{ij'} \mu_{j',\beta}^{\text{induc}}\right)$$
$$\text{with} \quad \alpha, \beta = 1, 2, 3 \tag{7}$$

where α_i is the atom polarizability, $E_{i,\alpha a}$ represents the electric fields generated by permanent multipoles and induced dipoles, $M_j = [q_j, \mu_{j1}, \mu_{j2}, \mu_{j3}, ...]^T$ includes the permanent multipole components, and $T_\alpha^{ij} = [T_\alpha, T_{\alpha 1}, T_{\alpha 2}, T_{\alpha 3}, ...]$ represents the matrix for the interaction of sites i and j, where $T_\alpha = \nabla_\alpha T = -(R_\alpha/R^3)$ and $T_{\alpha\beta} = \nabla_\alpha T_\beta$. The summations are carried out over two sets: $\{j\}$, all atom sites outside the molecule containing atom site i, and $\{j'\}$, all atom sites other than i. The function for the induced dipoles self-consistently reduces to

$$\mu_{i,\alpha}^{\text{induc}}(n+1) = \mu_{i,\alpha}^{\text{induc}}(n) + \alpha_i\left(\sum_{\{j\}} T_{\alpha\beta}^{ij'} \mu_{j',\beta}^{\text{induc}}(n)\right)$$
$$\text{with} \quad n = 0, 1, 2, ... \tag{8}$$

From this solution, the first term in eq 8 represents the direct induced dipole for atom i as a result of the electric field generated from the permanent multipoles from neighboring molecules. The second term represents the mutual induced dipole resulting from induced dipoles induced on all other atom sites. The mutual induction calculation is iterated until the induced dipoles are no longer induced by dipoles on all other sites with a tolerance set to 10^{-5} D.

For the reparameterization of the AMOEBA functional form, there were 21 tunable parameters included in the optimization: the vdW radius (R) and potential well depth (ε) for oxygen and hydrogen, reduction factor for hydrogen, bond-stretching force constant (K_b) and length (b), angle-bending force constant (K_θ) and magnitude (θ), Urey–Bradley force constant (K_l) and length (l), charge for hydrogen and oxygen, multipoles (dipole, quadrupole) for hydrogen and oxygen, polarizability for hydrogen and oxygen, and Thole polarization damping factor.

Simulation Protocol. Initial cycles of ForceBalance used a cubic box with an initial side length of 18.65 Å and containing 216 water molecules. Molecular dynamics in the NPT ensemble was performed via a Martyna–Tuckerman–Klein integrator incorporating a Nosé–Hoover thermostat and barostat.[54] Final liquid parameter optimization cycles were also done on 216 waters. Each final simulation was run for 4 ns following 400 ps of equilibration. The simulations for the final parametrization employed Langevin dynamics with a multiple time step velocity Verlet integrator with the Langevin friction force and random force. The Langevin dynamics used a friction coefficient of 1.0 ps^{-1}. These final simulations used a Monte Carlo barostat with a trial frequency of 1 box size change per 25 MD steps. All dynamics simulations were performed with either the TINKER[55] or OpenMM[56] modeling software packages. Properties, including the self-diffusion constant, viscosity, dielectric constant, enthalpy of vaporization, heat capacity, isothermal compressibility, and second virial coefficient, were computed by the same methods used for the earlier AMOEBA03 water model.[49]

Calibration Data. The data utilized for fitting the parameters was composed of a combination of experimentally determined condensed phase properties as well as robust *ab initio*-derived properties. The condensed phase properties considered were the density, enthalpy of vaporization, isothermal compressibility, isobaric heat capacity, thermal expansion coefficient, and dielectric constant. The temperature and pressure combinations were 1 atm at temperatures ranging from 249 to 373 K (32 total) and 298 K at pressures from 1 to 8 kbar (8 total). The complete lists of temperatures, pressures, and values for each experimental property are included in the Supporting Information.

The *ab initio* reference data included properties for systems ranging in size from the monomer to clusters of 22 water molecules. For the monomer, the charge, dipole, quadrupoles, polarizability, vibrations, and geometry were considered. The *ab initio* interaction energies and ground state geometries for the ground state dimer, Smith dimer set (10 total),[57] trimer, tetramer, pentamer, eight hexamers,[58] two octamers,[59] five 11-mers,[60] five 16-mers, two 17-mers, and four 20-mers[61,62] were utilized for calibration. In previous work,[63] over 42 000 cluster (ranging from 2 to 22 water molecules) geometries were obtained from AMOEBA simulations of liquid water for temperatures ranging from 249 to 373 K. Energies and gradients for the clusters were determined via RI-MP2[64,65]/heavy-aug-cc-pVTZ[66] as implemented in Q-Chem 4.0.[67] This large compilation of theoretical data was included in the fitting of the AMOEBA water parameters.

ForceBalance. The AMOEBA03 water model was parametrized by hand to fit results from *ab initio* calculations on gas phase clusters,[49] and temperature and pressure dependent bulk phase properties.[68] Here we apply ForceBalance, an automatic optimization method, to parametrize a revised AMOEBA14 model using the expanded data set described in the last section. ForceBalance has previously been applied to the development of a direct polarization variant of AMOEBA, labeled iAMOEBA, which omits the self-consistent calculation of polarization interactions.[63] One of the goals for iAMOEBA was to accurately describe bulk phase properties; therefore, the condensed phase properties, e.g., density, were given a greater weight than gas phase properties, such as cluster interaction energies. Ideally, the mutual AMOEBA model should be applicable across all system sizes and phases as well. To reflect this goal for the mutual polarization model, each property in the calibration set was initially given an equal weight. This is in contrast to the previous direct polarization water model, where the condensed phase experimental data was weighted more heavily than the gas phase cluster data.

The enthalpy of vaporization measures the water–water interaction strength, while the related property of the density reflects the hydrogen-bonded network structure, both of which have significant temperature (and pressure) dependence. If the enthalpy value is too large or its change with temperature is too steep, then the attraction between the water molecules is too great and the heat capacity would be too high. This would be problematic for not only the homogeneous water system but also in heterogeneous systems where the water–water, water–solute, and solute–solute interactions need to be balanced. For example, a temperature of maximum density (TMD) of a model that is very different than the experimental TMD would likely change the trends in hydrophobic hydration with temperature, since the entropic penalty for cavity formation in the liquid by definition changes with temperature. Therefore, the weighting of the condensed phase properties was adjusted to increase the weights of the enthalpy of vaporization and density in relation to the other condensed phase properties. The whole set of condensed phase properties maintained equal weighting with the gas phase data, but the individual condensed phase properties were assigned different weights with respect to each other.

DOI: 10.1021/jp510896n
J. Phys. Chem. B 2015, 119, 9423–9437

Table 1. AMOEBA Water Parameters for the AMOEBA03 and Revised AMOEBA14 Water Models and the Prior Widths Used in the ForceBalance Optimization Scheme

parameter	units	AMOEBA03	AMOEBA14	prior width
O monopole	e	−0.51966	−0.42616	0.4
O dipole *Z*	e bohr	0.14279	0.06251	0.1
O quadrupole *XX*	e bohr^2	0.37928	0.17576	0.2
O quadrupole *YY*	e bohr^2	−0.41809	−0.23160	0.2
O quadrupole *ZZ*	e bohr^2	0.03881	0.05584	0.2
H monopole	e	0.25983	0.21308	0.4
H dipole *X*	e bohr	−0.03859	−0.10117	0.1
H dipole *Z*	e bohr	−0.05818	−0.27171	0.1
H quadrupole *XX*	e bohr^2	−0.03673	0.12283	0.2
H quadrupole *YY*	e bohr^2	−0.10739	0.08950	0.2
H quadrupole *XZ*	e bohr^2	−0.00203	−0.06989	0.2
H quadrupole *ZZ*	e bohr^2	0.14412	−0.21233	0.2
O polarizability	Å	0.837	0.920	0.1
H polarizability	Å	0.496	0.539	0.1
damping factor	Å	0.39	0.39	none
O vdW diameter	Å	3.405	3.5791	0.3
O vdW epsilon	kcal/mol	0.11	0.1512	0.1
H vdW diameter	Å	2.655	2.1176	0.3
H vdW epsilon	kcal/mol	0.0135	0.0105	0.1
H vdW reduction factor	none	0.91	0.8028	0.1
O−H bond length	Å	0.9572	0.9565	0.1
bond force constant	kcal/mol/Å^2	556.85[a]	556.82	50
H−O−H angle value	degree	108.5	107.91	5
angle force constant	kcal/mol/rad^2	48.7[a]	48.98	40
H−H Urey−Bradley length	Å	1.5326[a]	1.5467	none
Urey−Bradley force const.	kcal/mol/Å^2	−7.6[a]	−8.62	25

[a]Current AMOEBA03 bond angle and Urey−Bradley intramolecular parameters. These values differ from those originally published in ref 49, and were changed to correct an error in the ordering of the O−H stretch vibrational modes.

ForceBalance supports many different optimization algorithms, and the calculation in this work was carried out using the trust-radius Newton−Raphson (or Levenberg−Marquardt[69,70]) algorithm with an adaptive trust radius.[71,72] This algorithm requires the first and second derivatives of the objective function in the parameter space, which we derive from the first derivatives of the simulated properties using the Gauss−Newton approximation.

A major challenge in force field parametrization is the significant statistical noise in the objective function from the sampling of properties to be matched to experiment. The parametric derivatives are challenging to evaluate because numerical differentiation requires running multiple simulations and evaluating small differences between statistically noisy estimates. ForceBalance uses thermodynamic fluctuation formulas to calculate accurate parametric derivatives of simulated properties without running expensive multiple simulations.[47,73] For instance, the ensemble average of a generic observable A that does not depend explicitly on the force field parameters (for example, the density or an order parameter) can be expressed as follows

$$\langle A\rangle_\lambda = \frac{1}{Q(\lambda)}\int A(\mathbf{r}, V)\exp(-\beta(E(\mathbf{r}, V; \lambda) + PV))\,\mathrm{d}\mathbf{r}\,\mathrm{d}V$$
$$Q(\lambda) = \int \exp(-\beta(E(\mathbf{r}, V; \lambda) + PV))\,\mathrm{d}\mathbf{r}\,\mathrm{d}V \tag{9}$$

where A is the observable, $\mathbf{r}$ a given molecular configuration in a periodic simulation cell, λ the force field parameter, E the potential energy, $\beta \equiv (k_\mathrm{B}T)^{-1}$ the inverse temperature, k_B the Boltzmann constant, T the temperature, P the pressure, V the volume, and Q the isothermal−isobaric partition function and the angle brackets with a λ subscript represent an ensemble average in the thermodynamic ensemble of the force field parametrized by λ. In practice, this integral is evaluated numerically using molecular dynamics or Monte Carlo simulation in the NPT ensemble.

Since the expression for A depends on λ only through the potential energy E, we can differentiate eq 9 analytically:

$$\frac{\mathrm{d}}{\mathrm{d}\lambda}\langle A\rangle_\lambda = \frac{1}{Q(\lambda)}\int A(\mathbf{r}, V)\exp(-\beta(E(\mathbf{r}, V; \lambda) + PV))\left(-\beta\frac{\mathrm{d}E(\mathbf{r}, V)}{\mathrm{d}\lambda}\right)\mathrm{d}\mathbf{r}\,\mathrm{d}V - \frac{1}{Q(\lambda)^2}\frac{\mathrm{d}Q}{\mathrm{d}\lambda}\int A(\mathbf{r}, V)\exp(-\beta(E(\mathbf{r}, V; \lambda) + PV))\,\mathrm{d}\mathbf{r}\,\mathrm{d}V$$
$$= -\beta\left(\left\langle A\frac{\mathrm{d}E}{\mathrm{d}\lambda}\right\rangle_\lambda - \langle A\rangle_\lambda\left\langle\frac{\mathrm{d}E}{\mathrm{d}\lambda}\right\rangle_\lambda\right) \tag{10}$$

The potential energy derivative $\langle \mathrm{d}E/\mathrm{d}\lambda\rangle$ is evaluated by numerically differentiating the potential energies at the sampled structures. Equation 10 provides a way to evaluate the parametric derivative of thermodynamic properties without running additional sampling simulations, though the derivative of any observable always manifests as a higher order correlation function and has a larger statistical error than the observable itself. This equation may be directly applied to obtain derivatives of ensemble-averaged observables with implicit parametric dependence through the thermodynamic ensemble, such as the

DOI: 10.1021/jp510896n
J. Phys. Chem. B 2015, 119, 9423−9437

density ρ. Equation 10 is easily extensible to obtain derivatives of observables with explicit parameter dependence, such as the enthalpy; derivatives for higher-order thermodynamic response properties such as the dielectric constant are obtained using the chain rule.[63] We omit the calculation of second parametric derivatives for reasons of computational cost and statistical noise, relying instead on the least-squares form of the objective function and the Gauss−Newton approximation to obtain the Hessian.

In order to maximize the efficiency of simulating properties, ForceBalance interfaces with several powerful and complementary technologies. ForceBalance includes interfaces to AMOEBA via the TINKER[55] modeling software and via OpenMM 6.1,[56] a graphics processing unit (GPU)-accelerated MD engine. The Work Queue library[74] allows ForceBalance to parallelize multiple simulations across compute nodes in different physical locations. ForceBalance analyzes the data from finished simulations using the multistate Bennett acceptance ratio estimator (MBAR)[75] which allows multiple simulations at different thermodynamic phase points to statistically contribute to one another. All of these software packages and methods are freely available on the Web.

The problem of overfitting is treated by regularization via a penalty function, which corresponds to imposing a *prior* distribution of parameter probabilities in a Bayesian interpretation. The prior widths reflect the expected variations of the parameters during the optimization, which may be chosen heuristically or sampled over in an empirical Bayes approach. Our optimization was regularized using a Gaussian prior specified in Table 1, corresponding to a parabolic penalty function in parameter space centered at the original AMOEBA parameter values with the chosen force constants. Since the various parameters have different physical meanings (e.g., vdW well depth, O−H bond length), each parameter type was assigned its own prior width.

We ran the optimization until fluctuations from numerical noise prevented further improvement. The calculation converged to within the statistical error after about 10 nonlinear iterations, though we performed several optimizations with different choices of weights for the reference data and prior widths before arriving at the final answer.

RESULTS AND DISCUSSION

AMOEBA14 Water Parameters. The parameters for the new AMOEBA14 water model, the AMOEBA03 model, and the Gaussian prior widths included in the ForceBalance optimization are reported in Table 1. The prior widths are proportional to the inverse-squared strength of the harmonic penalty for each parameter and reflect the parameter's intrinsic size and expected variability. It should be noted that the bond force constant, angle force constant, and Urey−Bradley parameters for AMOEBA03 were modified in 2013 when it was observed that the original parameters incorrectly predicted the order of the vibrational frequencies; therefore, the comparison we are making for intramolecular parameters is to those revised parameters. Table 1 shows that the intramolecular parameters for the AMOEBA model remained essentially unchanged from 2003 to 2014.

The damping value of 0.39 was kept fixed during the AMOEBA14 model optimization, since the value in the 2003 model was set based on water cluster energies, and this damping value has been tested and employed for the majority of atom classes within the AMOEBA model. For the AMOEBA03 water model, the polarizability parameters for oxygen and hydrogen were those proposed by Thole. While the polarizability values were allowed to fluctuate during the ForceBalance optimization of AMOEBA14, they do not deviate significantly from the AMOEBA03 model.

Repulsion-dispersion parameters (vdW radius and well-depth) were assigned to both the oxygen and hydrogen atom centers. AMOEBA14 has a larger vdW radius and well-depth for oxygen and a smaller vdW radius and well-depth for hydrogen compared to AMOEBA03. The newly proposed reduction factor for hydrogen shifts the hydrogen vdW center toward oxygen by approximately 20% of the O−H bond length. The parameter optimization approached a point of zeroing out the hydrogen vdW site and reducing the model to one repulsion-dispersion site on oxygen, but the final set of parameters includes both atoms and the description of the water oxygen is consistent with the description of oxygen in other organic molecules for the AMOEBA model.

The AMOEBA14 water model increases the charge of the oxygen and decreases the charge of the hydrogen in comparison to the AMOEBA03 model. The *z*-component of the oxygen dipole is less than AMOEBA03, and the *x*- and *z*-components of the hydrogen dipole are greater. There are substantial deviations for both the oxygen and hydrogen quadrupole parameters in relation to the AMOEBA03 model. The *xx*-component of the quadrupole moment tensor decreases by approximately the same magnitude by which the *yy*-component of the quadrupole increases for oxygen. An increase of the same scale is observed for the *xx*- and *yy*-components of the quadrupole moment tensor for hydrogen, but there is a sign change for these hydrogen quadrupole parameters. These changes in the nonbonded interactions reflect improvements in the gas phase and condensed phase properties of water described in the next sections.

AMOEBA14 Fitted Gas Phase Water Properties. Table 2 provides the multipole properties predicted by the AMOEBA14 and AMOEBA03 water models. The AMOEBA14 water parameters predict the dipole of a gas phase water monomer to be 1.808 D in comparison to the experimental value of 1.855 D. The changes in the atomic quadrupole parameters improve the molecular *xx*-quadrupole moment compared to experiment, while the *yy*- and *zz*-quadrupole moments are nearly unchanged in comparison to the AMOEBA03 model.

Table 2. Multipole Properties Predicted by the Revised AMOEBA14 and Previous AMOEBA03 Water Models Compared to Experimental Values[a]

	AMOEBA03	AMOEBA14	experiment
dipole d_z	1.771	1.808	1.855[b]
	Quadrupole		
Q_{xx}	2.502	2.626	2.630[c]
Q_{yy}	−2.168	−2.178	−2.500[c]
Q_{zz}	−0.334	−0.045	−0.130[c]
	Polarizability		
α_{xx}	1.672	1.767	1.528[d]
α_{yy}	1.225	1.308	1.412[d]
α_{zz}	1.328	1.420	1.468[d]

[a]Units are D, D·A, and $A^2 \cdot s^4 \cdot kg^{-1}$, respectively. [b]Reference 110. [c]Reference 111. [d]Reference 112.

As in the original AMOEBA model, the ideal bond angle is larger than the experimental and ab initio values. The three vibrational frequencies of the water monomer are predicted to within 0.3 cm^{-1}, and the ordering of the modes is in agreement with experiment. In Table 3, the AMOEBA water dimer

DOI: 10.1021/jp510896n
J. Phys. Chem. B 2015, 119, 9423−9437

Table 3. Dimer Equilibrium Properties: Dissociation Energy (D_e, kcal/mol), O−O Distance (r_{O-O}, Å), α Angle (Angle between the O−O Vector and the $O_{donor}-H_{donor}$ Vector, deg), β Angle (Angle between the O−O Vector and the Plane of the Acceptor Molecule, deg), and Total Dipole Moment (μ_{tot}, D)

property	AMOEBA03	AMOEBA14	*ab initio*	experiment
D_e	4.96	4.64	4.98[c]	5.44 ± 0.7[a]
r_{O-O}	2.892	2.908	2.907[c]	2.976[b]
α	4.18	4.41	4.18[c]	−1 ± 10[b]
β	57.2	64.9	55.6[d]	57 ± 10[b]
μ_{tot}	2.54	2.20	2.76[e]	2.643[b]

[a]Reference 113. [b]Reference 114. [c]Reference 115. [d]Reference 116. [e]Reference 117.

equilibrium structure and interaction energy are compared to experiment and *ab initio* results. For the equilibrium dimer minimum, the AMOEBA14 model is in somewhat poorer agreement with *ab initio* values than the earlier AMOEBA03 model. However, averaged over a series of low energy dimer configurations, AMOEBA14 is as good as or superior to AMOEBA03. As previously noted, 10 *ab initio* dimer interaction energies and geometries were including in the fitting of the model parameters. The root mean squared deviations (RMSDs) for the monomer and dimer geometries were 0.017 and 0.057 Å, respectively.

The interaction energies for water clusters, ranging from dimers to clusters of 20 water molecules (see Table 4), were analyzed with the AMOEBA water model. The geometries of the clusters were optimized and the interaction energy determined via AMOEBA. The cluster results are compiled in Table 4. The mean absolute deviation (MAD) for the interaction energy of the smaller clusters (2−8 water molecules) is 0.39 kcal/mol, considered to be within chemical accuracy (i.e., within 1 kcal/mol of experiment). Specific results for the hexamers are shown in Figure 2. The larger clusters (11- to 20-mers) have an MAD of 7.97 kcal/mol for the interaction energy prediction. The discrepancy between the accuracy levels of the AMOEBA water model for the small and large clusters is interesting and would suggest the error of AMOEBA with respect to system size could be systematic. To examine this possibility, the MADs of each of the condensed phase properties (discussed further below) were tabulated in Table 5, and the errors were of the same magnitude as the small clusters.

In the analysis of the 42 000 clusters (~2400 clusters of n water molecules, n = 2−22), the potential energies, gradients, net forces, and torques were computed with AMOEBA14 and compared to the *ab initio* reference data. As a specific example of the results, the root mean squared (RMS) errors for the cluster of 18-mers were 7.8 kJ/mol (10%) for the energy, 33.8 kJ/mol/Å (42%) for the gradient, 9.9 kJ/mol/Å (30%) for the net force, and 6.3 kJ/mol/rad (25%) for the torque. The standard deviations for the reference data were 29.2 kJ/mol, 83 kJ/mol/Å, 29 kJ/mol/Å, and 20 kJ/mol/rad for the energies, gradients, forces, and torques, respectively. Over all of the cluster sizes, the AMOEBA14 model predicted the potential energies to, on average, within 15% of the reference. This accuracy level is surprising when the weighting of the reference data is considered. The bulk clusters were assigned the smallest weights; i.e., fitting the energies and gradients was the lowest priority in the parameter optimization. The robustness of the AMOEBA14 model in comparison to *ab initio* cluster reference data reaffirms the utility of the model for both gas and bulk phase properties.

Table 4. Cluster Binding Energies (kcal/mol) with the AMOEBA14 Model in Comparison to *Ab Initio* Reference Calculations[a]

	molecule	ref	AMOEBA14	diff
dimers[b] (Smith)	**1**	−4.968	−4.65	0.32
	2	−4.453	−4.22	0.24
	3	−4.418	−4.19	0.23
	4	−4.25	−3.54	0.71
	5	−3.998	−3.06	0.94
	6	−3.957	−2.92	1.04
	7	−3.256	−2.49	0.77
	8	−1.3	−1.02	0.28
	9	−3.047	−2.37	0.68
	10	−2.182	−1.96	0.22
	trimer[c]	−15.742	−15.38	0.36
	tetramer[c]	−27.4	−27.43	−0.03
	pentamer[c]	−35.933	−35.78	0.16
hexamer[d]	prism	−45.92	−45.18	0.74
	cage	−45.67	−45.83	−0.16
	bag	−44.3	−44.52	−0.22
	cyclic chair	−44.12	−43.53	0.59
	book A	−45.2	−45.08	0.12
	book B	−44.9	−45.06	−0.16
	cyclic boat A	−43.13	−42.99	0.14
	cyclic boat B	−43.07	−43.07	0.00
octamer[e]	S_4	−72.7	−72.22	0.48
	D_{2d}	−72.7	−72.24	0.46
11-mer[f]	434	−105.718	−101.11	4.61
	515	−105.182	−100.99	4.19
	551	−104.92	−100.58	4.34
	443	−104.76	−101.17	3.59
	4412	−103.971	−100.33	3.64
16-mer[g]	boat A	−170.8	−160.45	10.35
	boat B	−170.63	−160.39	10.25
	antiboat	−170.54	−160.30	10.25
	ABAB	−171.05	−161.20	9.85
	AABB	−170.51	−160.89	9.62
17-mer[g]	sphere	−182.54	−171.53	11.01
	5525	−181.83	−170.42	11.41
20-mer[h]	dodecahedron	−200.1	−193.81	6.29
	fused cubes	−212.1	−205.77	6.33
	face-sharing prisms	−215.2	−204.41	10.79
	edge-sharing prisms	−218.1	−207.06	11.04
		MAD	units	
clusters	dimer to octamer	0.39	kcal/mol	
	11- to 20-mer	7.97	kcal/mol	

[a]Mean absolute deviations (MADs) are reported over the small and large cluster categories. [b]Reference 118. [c]Reference 49. [d]Reference 58. [e]Reference 59. [f]Reference 60. [g]Reference 119. [h]Reference 61.

The second virial coefficient of water computed with an empirical potential is a sensitive measure of the accuracy of the Boltzmann-weighted dimer potential energy surface. Following Millot et al., we computed the classical virial coefficient, as well as first-order translational and rotational quantum corrections.[76] Some workers have argued that the quantum corrections are unnecessary, as they are implicitly incorporated into empirical water potentials.[77] Others have emphasized the importance of higher-order corrections and experimental error, especially at temperatures below about 325 K.[78] Figure 3 shows both the

DOI: 10.1021/jp510896n
J. Phys. Chem. B 2015, 119, 9423−9437

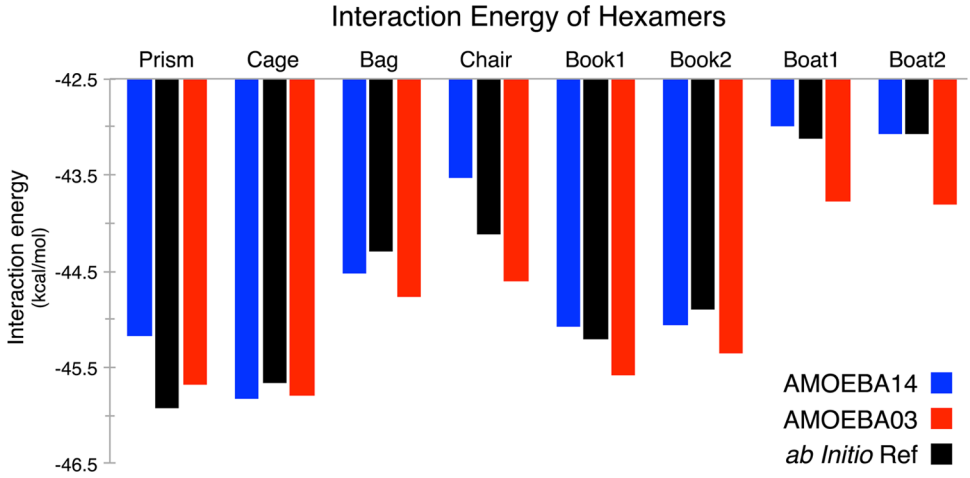

Figure 2. Energies of water hexamer minima for the AMOEBA03 and AMOEBA14 models compared to reference complete basis set (CBS) *ab initio* calculations from ref 58.

Table 5. Mean Absolute Deviations (MADs) from Experiment of the Liquid Phase Properties Calculated by AMOEBA14 across All Temperatures (249−373 K)

property	MAD	units
ρ	1.22	kg/m^3
ΔH_{vap}	0.43	kJ/mol
α	0.66	10^{-4}/K
κ_T	1.31	10^{-6}/bar
C_p	2.28	cal/mol/K
$\varepsilon(0)$	1.51	N/A

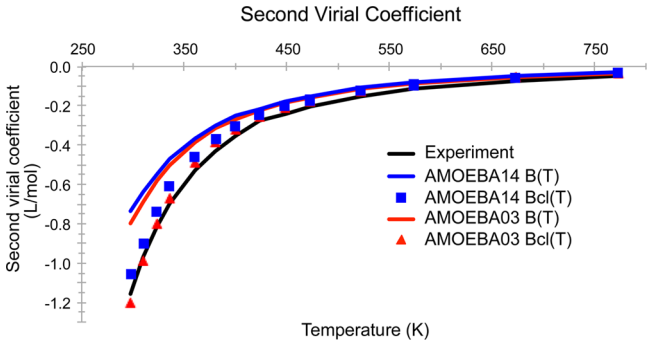

Figure 3. Second virial coefficient of water as a function of temperature for the AMOEBA03 and AMOEBA14 models for temperatures from 249 to 373 K and atmospheric pressure (1 atm). The Bcl(T) curves show the classical second virial coefficient, while the B(T) curves have translational and rotational quantum corrections added to the classical results. Experimental values are from refs 124 and 125.

classical and first-order corrected second virial coefficients for the AMOEBA03 and AMOEBA14 models. The two models exhibit very similar behavior, and in both cases, the uncorrected coefficients are in excellent agreement with experiment. Nonpolarized models intended for use in the bulk phase simulation tend to lie below the experimental second virial curve, especially at low temperature. The iAMOEBA model (not shown) is also somewhat underpolarized, and also yields second virial coefficients that are too negative.

In previous work,[25] the dependence of the density maximum on the water geometry was explored. The 2003 model adopted an equilibrium angle of 108.5° in the gas phase ("correct" value per *ab initio*: 104.5°) in order to achieve an average angle of 105.3° in the condensed phase and be in near agreement with experiment at room temperature. With the reoptimized AMOEBA parameters, the equilibrium gas phase angle is 107.8° and the condensed phase angle is 105.1°. The average AMOEBA14 H−O−H angle slightly increases (104.9 to 105.4°) as the temperature increases from 249 to 373 K. While previous theoretical estimates concluded the liquid water should see the angle contract with increasing temperature,[79] experimental data has reported no relation between angle magnitude and temperature.[80]

AMOEBA14 Fitted Condensed Phase Water Properties. In the parametrization of the initial AMOEBA03 water model, only the density and heat of vaporization at room temperature were considered. Within the fitting of the current model, six condensed phase properties were considered at a range of temperatures (249−373 K) and pressures (1 atm to 8 kilobar). For AMOEBA14, the enthalpy of vaporization and density trends with temperature were the focal points in the fit and were given a greater weight in the optimization. All of the thermodynamic data and their trends with respect to temperature are shown in Figures 2−5, while tables with the raw numbers are included in the Supporting Information.

Since AMOEBA03 was specifically fit to the enthalpy of vaporization and the density at room temperature, the initial model agrees with the corresponding experimental values to within statistical error. However, the linear temperature dependence of the enthalpy of vaporization only intersects with the experiment at room temperature. With the AMOEBA14 water model, the enthalpy of vaporization at room temperature differs by only 0.49 kcal/mol over the temperature range examined, and the mean absolute deviation (MAD) of the model was 0.43 kcal/mol compared to 0.65 for AMOEBA03 (Figure 4). The experimental maximum density of 999.972 kg/m^3 occurs at 277.15 K and 1.0 atm of pressure. The temperature of maximum density as predicted by the AMOEBA03 model is shifted to higher temperatures by nearly 15 K, and the curve of the temperature dependence is slightly narrower. The new AMOEBA14 water parameters yield a temperature of maximum density in quantitative agreement with experiment, and the shape of the curve is in qualitative agreement with experiment (Figure 5).

The AMOEBA14 results for the thermodynamic fluctuation properties (heat capacity, isothermal compressibility, and

DOI: 10.1021/jp510896n
J. Phys. Chem. B 2015, 119, 9423−9437

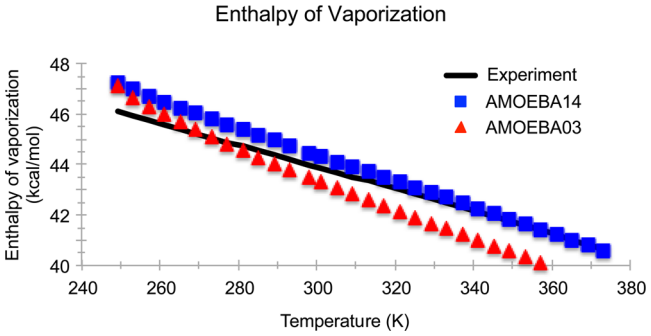

Figure 4. Enthalpy of vaporization of water for temperatures for the AMOEBA03 and AMOEBA14 models and experiment for temperatures from 249 to 373 K and atmospheric pressure (1 atm). The mean signed deviation is −0.43 kcal/mol. Experimental values are from ref 120.

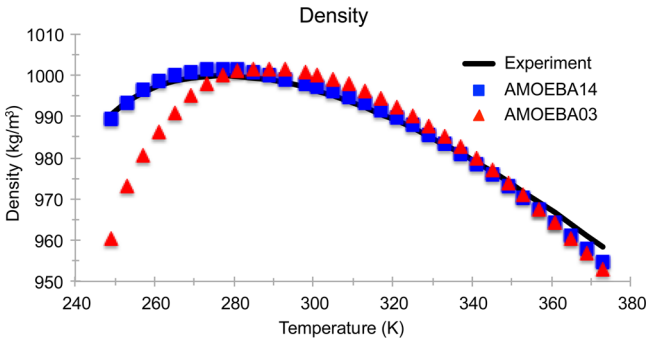

Figure 5. Density of water for the AMOEBA03 and AMOEBA14 models compared to experiment for temperatures from 249 to 373 K at atmospheric pressure (1 atm). The temperature of maximum density from experiment and for AMOEBA14 is 277 K. Experimental values are taken from ref 126.

thermal expansion coefficient) are shown in Figures 6−9. Since the temperature dependence of the predicted enthalpy of

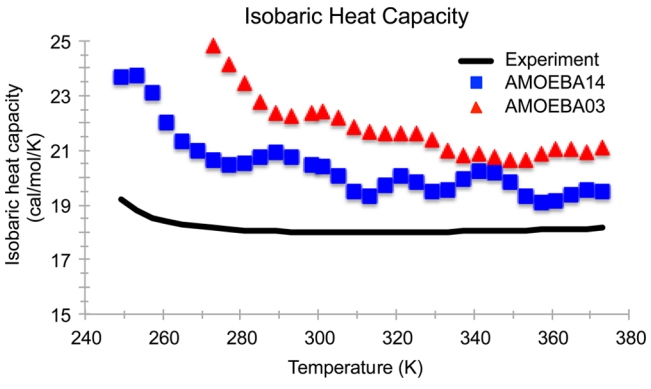

Figure 6. Isobaric heat capacity for the AMOEBA03 and AMOEBA14 models compared to experiment for temperatures from 249 to 373 K at atmospheric pressure (1 atm). Experimental values are taken from ref 120.

vaporization has a slightly greater slope than experiment (Figure 4), the calculated heat capacity for AMOEBA14 is greater than experiment by, on average, 2.28 cal/mol/K. AMOEBA14 improves upon the AMOEBA03 model, whose enthalpy of vaporization temperature dependence is much steeper, resulting in much higher heat capacity values. The discrepancy between the AMOEBA14 calculated and experimental heat capacity is due to the approximations within our classical, flexible model, and previous work has estimated the accuracy of the heat capacity determined by AMOEBA to be ±5 cal/mol/K.[25] While an overestimation of the heat capacity means an overestimation of the entropy fluctuations, what matters more is that the temperature onset of anomalous fluctuations (i.e., above the normal background) is better described by the AMOEBA14 model relative to AMOEBA03 (Figure 6).[81]

The AMOEBA14 model also shows a drastic improvement in the quantitative value of the isothermal compressibility in comparison to the 2003 model, which overestimates the compressibility by ∼30% under ambient conditions. Again, the more important point is that the temperature trends are correct for AMOEBA14, with a compressibility minimum very near the 319 K value seen experimentally (Figure 7). AMOEBA14 not

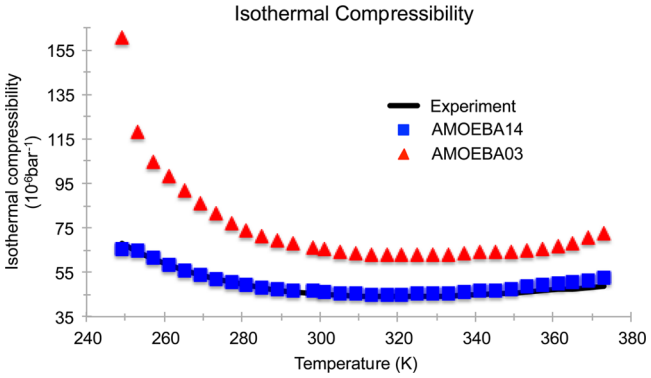

Figure 7. Isothermal compressibility for the AMOEBA03 and AMOEBA14 models compared to experiment for temperatures from 249 to 373 K at atmospheric pressure (1 atm). Experimental values are taken from ref 126.

surprisingly shows the transition from positive to negative thermal expansion coefficient at the same temperature as experiment, which is to be expected given that the TMDs are the same (Figure 8).

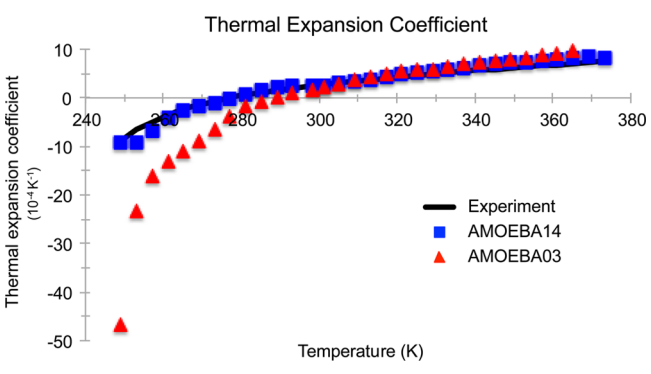

Figure 8. Thermal expansion coefficient for the AMOEBA03 and AMOEBA14 models compared to experiment for temperatures from 249 to 373 K at atmospheric pressure (1 atm). Experimental values are from ref 126.

Finally, Figure 9 shows the temperature dependence of the dielectric constant, which is in excellent agreement with experiment, and also agrees well with the AMOEBA03 value of ∼80 at room temperature. The excellent reproduction of the dielectric constant for the AMOEBA14 model is due to a good balance within the electrostatic model. Carnie and Patey showed

DOI: 10.1021/jp510896n
J. Phys. Chem. B 2015, 119, 9423−9437

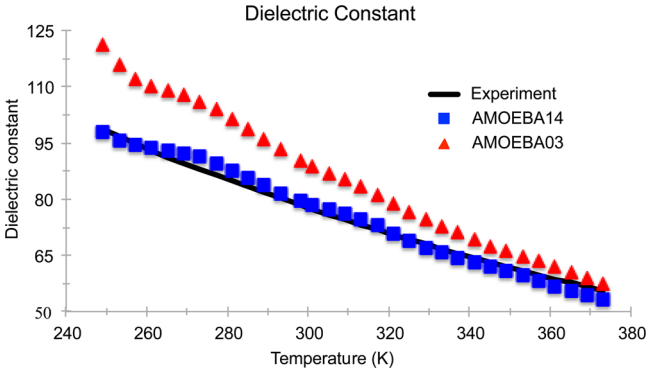

Figure 9. Dielectric constant for the AMOEBA03 and AMOEBA14 models compared to experiment for temperatures from 249 to 373 K at atmospheric pressure (1 atm). Experimental values are taken from ref 120.

the dipolar correlations are suppressed when the quadrupole interactions increase, thereby decreasing the dielectric constant of the liquid.[82] It has been noted[83] that, since the dielectric response arises from both the magnitude as well as the fluctuations of the water dipole, by definition, a good dielectric constant can be achieved by a model with either small dipoles with large fluctuations (corresponding to small quadrupoles $< \sim 1.8$ D-Å) or large dipoles with small fluctuations (large quadrupoles $> \sim 2.5$ D-Å). It appears, therefore, that the polarization of the AMOEBA models give rise to dipoles that are large enough to overcome the quadrupolar quenching in achieving its excellent dielectric properties.

AMOEBA14 Validation. *Radial Distribution Function.* The radial distribution functions (RDFs) can be derived from X-ray scattering and neutron diffraction[84,85] and provide information about the structure of liquid water. Figure 10 shows the oxygen−oxygen RDF curve of the AMOEBA03, AMOEBA14, and iAMOEBA models when compared against the ALS[86] and more recent APS[87] experimental estimates of the real space structure derived from the intensity data. The $g_{OH}(r)$ and $g_{HH}(r)$ curves are included in the Supporting Information. The AMOEBA14 model is in overall good agreement with experiment for the three

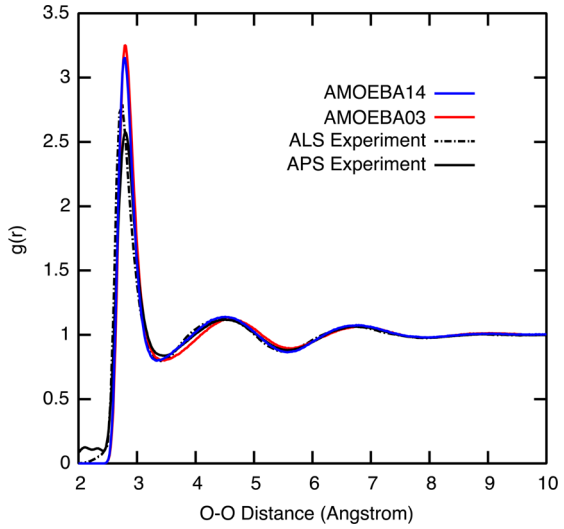

Figure 10. Water oxygen−oxygen radial distribution functions at 298 K for AMOEBA03, AMOEBA14, and iAMOEBA compared against experimental values from refs 86−88.

distributions. The height of the first peak in $g_{OO}(r)$ is approximately 0.4 and 0.6 greater than the ALS and APS X-ray data, respectively, but the location of the peak is at the same oxygen−oxygen distance as experiment. The first and second troughs, as well as the second peak, of the $g_{OO}(r)$ nearly overlap the experimental curve, with deviations of less than 0.1%. A similar level of agreement is seen between the AMOEBA models and experiment for the $g_{OH}(r)$ and $g_{HH}(r)$, and as an effective potential, it probably captures, imperfectly, any nuclear quantum effects. Prior path integral and classical MD simulations of flexible water models, such as for TIP4F,[32] suggest the first $g_{OO}(r)$ peak is reduced in height and shifted to a slightly larger distance in the path integral calculations.

Assuming a model for the condensed phase water electron density based on modified atomic form factors (MAFFs),[86] we can Fourier transform the radial distribution functions to derive a simulated intensity curve to compare against the ALS[88] and APS[87] intensity data (Figure 11). Since the RDFs were not

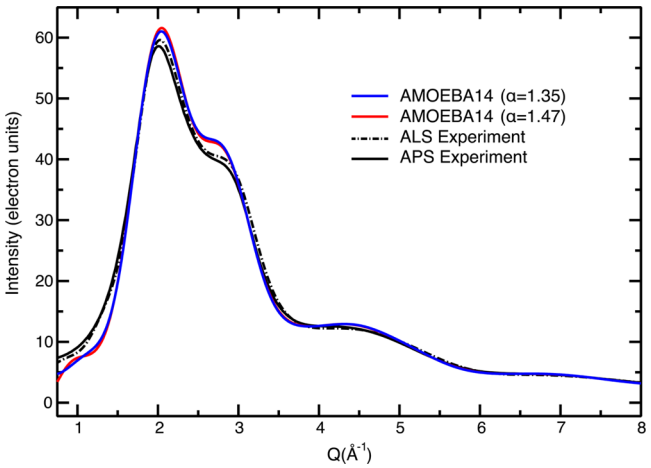

Figure 11. Comparison of the ALS and APS experimental X-ray scattering intensities from refs 87 and 88 for liquid water at 1 bar and 298 K with curves simulated with AMOEBA14 models modified to have molecular polarizabilities of α = 1.47 Å^3 and α = 1.35 Å^3.

included in the calibration data, we performed three optimizations with different molecular polarizability targets (1.35, 1.41, and 1.47 Å^3) to determine its effect on water structure. The lower bound is based on an earlier *ab initio* calculation that suggested a reduction in the molecular polarizability in going from the gas phase (1.47 Å^3) to the condensed phase (1.35 Å^3).[89] More recent work has evaluated the molecular polarizability in the liquid using a different method, and determined that it was not significantly different from the gas phase value.[90] It is evident from Figure 11 that modifying, within reason, the polarizability produced no qualitative difference in the RDFs, although other properties may be sensitive to other water properties, though we do not investigate them here. Overall, the AMOEBA model intensities fall outside the differences between the ALS and APS experiments, which is likely a result of the larger first peak in the $g_{OO}(r)$ compared to experimental estimates.

Electrostatic Potential. The general protocol in the development of novel AMOEBA parameters typically optimizes the atomic multipole parameters by fitting to the molecular electrostatic potential generated via a gas phase *ab initio* molecular orbital calculation.[50] As detailed above, the AMOEBA14 water multipole parameters were allowed to

DOI: 10.1021/jp510896n
J. Phys. Chem. B 2015, 119, 9423−9437

fluctuate in conjunction with the remaining parameters and the monomer electrostatic potential map was not included in the fitting. The TINKER POTENTIAL program was used to compare the electrostatic potential for a single water molecule on a dense, uniform grid of points in a band 1.0−2.05 Å from the vdw surface. The average magnitude for the electrostatic potential from an MP2/aug-cc-pVQZ calculation was 6.6851 kcal/mol/e−, and the deviations for AMOEBA03 and AMOEBA14 were found to be −0.0499 and −0.0584. While the AMOEBA14 model was not fit to the *ab initio* electrostatic potential, the model is clearly effective for gas phase calculations outside of the calibration data.

Transport and Surface Tension Properties at Room Temperature. The viscosity, self-diffusion constant, and surface tension at room temperature were computed for the AMOEBA14 model. Viscosity was computed via the Einstein−Helfand relation and using the off-diagonal components of the pressure tensor. The viscosity of AMOEBA14 is 0.900 centipoise (cP) and is in nearly perfect agreement with the experimental measurement of 0.896 cP at 298 K.[91] Self-diffusion was computed via the Einstein equation via average motion over all molecules across a full MD simulation. The standard self-diffusion coefficient as determined from an NPT simulation with 216 molecules in a periodic box is 1.99×10^{-5} cm^2/s, which underestimates the experimental self-diffusion coefficient of 2.29×10^{-5} cm^2/s. Yeh and Hummer have suggested an analytical system-size correction for diffusion coefficients computed via periodic MD simulation.[92] Application of their correction increases the AMOEBA14 value to 2.36×10^{-5} cm^2/s. Diffusion is a key property where the importance of QNE is widely debated. Recently, Habershon et al. have extensively compared RPMD and classical simulation of water, and concluded that quantum fluctuations only increase the translational diffusion rate by a factor of 1.15.[35] This relatively small rate increase results from competing effects of intra- and intermolecular zero point energy, which increase the monomer dipole moment and destabilize the hydrogen bonding network, respectively. The surface tension computed via averaging over the diagonal elements of the pressure tensor is γ = 69.21 N/m, and deviates less than 0.5% from the corresponding experimental value determined at 298 K.[93] All of these properties are summarized in Table 6.

Ion−Water Interactions. It is important to validate the AMOEBA14 water model for not only a homogeneous system but also a heterogeneous system. The ion−water interaction was examined for the gas phase dimer system and the ion hydration free energy. The ions considered were the sodium cation (r = 2.85, ε = 0.15, α = 0.12) and chloride anion (r = 4.20, ε = 0.5, α = 4.0). Ion hydration free energies were computed via the orthogonal space random walk (OSRW) method.[94] The binding energies and equilibrium distance for the ion−water dimer and the ion hydration free energies are reported in Table 6. The AMOEBA14 model predictions for the ion−water dimer interaction energies are within 0.5 kcal/mol of experiment, while the ion hydration free energies are slightly overestimated for both the anion and the cation. Since water−ion intermolecular interactions are large and involve significant polarization, it is encouraging that the ion parameters required only a minor adjustment from the 2003 values[25] for use with AMOEBA14. While much further testing is necessary, this holds promise that AMOEBA parameters for other systems will retain compatibility with the new AMOEBA14 water model.

Table 6. Miscellaneous Bulk Water Properties and Ion Solvation Free Energies for the AMOEBA14 Water Model[a]

property	expt	AMOEBA03	AMOEBA14	iAMOEBA
viscosity	0.896[c]	1.08	0.900	0.85
self-diffusion constant	2.29[d]	2.0	1.99	
size-corrected diffusion[b]		2.3	2.36	2.54
surface tension (300 K)	71.73[e]	64		68.3
surface tension (298 K)	71.97[e]		69.21	
Na^+ ΔG(hydration)	−86.8[f]	−89.9	−91.91	
Cl^- ΔG(hydration)	−87.2[f]	−84.6	−89.25	
Na^+−H_2O dimer distance	2.23[g]	2.232	2.252	2.47
Na^+−H_2O dissociation energy	−23.6[g]	−23.53	−23.23	−21.81
Cl^-−H_2O dimer distance	3.103[h]	3.151	3.147	2.965
Cl^-−H_2O dissociation energy	−15.4[h]	−15.99	−15.72	−18.11

[a]All energies are in kcal/mol. Distances are in Å, viscosity is in cP, and diffusion is in 10^{-5} cm^2/s. [b]Reference 92. [c]Reference 91. [d]Reference 120. [e]Reference 93. [f]Reference 121. [g]Reference 122. [h]Reference 123.

CONCLUSION

The inclusion of polarizability makes the AMOEBA model preferable over other fixed-charge water models when characterizing water at different state points, for asymmetric environments, and for better transferability. With the advances made in computational modeling over the past decade, the AMOEBA water model was revisited in order to calibrate the parameters against a large, diverse data set. The new AMOEBA water model improves in accuracy over the original model for the prediction of bulk properties over large temperature and pressure ranges, in addition to maintaining reliability for gas phase property determination. By utilizing the ForceBalance methodology to optimize the AMOEBA model, nearly two dozen parameters could be systematically fit to a data set of *ab initio* calculations and experimental measurements.

The new AMOEBA water model is an improvement over the previous model, since a range of temperatures and pressures, as well as more gas phase and bulk properties, were included in the fitting of the parameters. For the six condensed phase properties in the calibration data set, AMOEBA14 qualitatively matches the experimental curves over the temperature range and the deviations from experiment are generally within a reasonable error margin. The current model exactly matches the experimental temperature of maximum density and the enthalpy of vaporization at room temperature differs by less than 0.5 kcal/mol, with a mean absolute deviation of 0.43 kcal/mol over the temperature range studied. The improvement observed for the bulk phase prediction of the AMOEBA14 model does not come at the expense of the accuracy of the model for gas phase property determination. The AMOEBA14 model has a similar accuracy level as the AMOEBA03 model for the interaction energy of the gas phase cluster ranging from dimers to 20-mers. The integrity of the new model parameters holds for properties not included in the calibration data set, as evidenced by the good agreement observed between the experimental radial distribution functions for oxygen−oxygen, oxygen−hydrogen, and hydrogen−hydrogen and those obtained via AMOEBA14.

The development of the new AMOEBA14 parameters is significant for modeling systems solvated in water, where the

DOI: 10.1021/jp510896n
J. Phys. Chem. B 2015, 119, 9423−9437

balance of solvent−solvent, solvent−solute, and solute−solute interactions is crucial for determining solute behavior. Within this work, we have demonstrated the accuracy of the AMOEBA14 model for a heterogeneous system, specifically the calculation of ion hydration free energies. Future applications of the model, for example, determining ligand binding affinities, will benefit from the improved definition of the AMOEBA water parameters.

While the revised model reported here represents a clear improvement over the 2003 parametrization for the intended uses of AMOEBA, there are several missing features important for other applications of an empirical water potential. In particular, the AMOEBA model does not describe the coupling of electrostatics with the valence geometry, penetration effects related to the point-based electrostatic model, quantum nuclear effects, and the dissociability of water in the bulk phase.

When the bond lengths and bond angle of water change from their equilibrium gas phase values, the electrostatic potential changes in a fashion that is not fully accounted for by the translation of atomic charges or rotation of atomic multipoles in traditional biomolecular water models or AMOEBA. Palmo et al.[95] have proposed a simple charge flux treatment of electrostatic-valence coupling. Fanourgakis and Xantheas[96] have explicitly included the monomer dipole moment surface as a function of geometry in their TTM2 family of water models. The latter method is correctly able to describe the increase in the H−O−H angle on moving from the gas to bulk phase. Models that do not include this additional coupling term exhibit a decreased average bond angle value in the liquid compared to the equilibrium parameter value. For example, AMOEBA models require an equilibrium H−O−H angle value near 108° in order to generate an average angle value[80] of at least 105° in the liquid phase.

Most current generation water models are missing an explicit term to account for charge penetration effects. Such a term is needed to correct for the use of point charges, or point multipoles in the case of AMOEBA, restricted to nuclear positions. A variety of empirical and semiempirical damping functions have been proposed to treat penetration in the context of both molecular mechanics,[97−99] including the AMOEBA benzene dimer,[100] and QM/MM calculations.[101,102] We plan to explore how charge penetration effects within the AMOEBA model impact the water parametrization. For example, the preliminary indication is inclusion of charge penetration reduces the largest differences between *ab initio* and AMOEBA dimer energies (see Table 4).

The AMOEBA model attempts to implicitly account for quantum nuclear effects (QNEs) in the context of classical simulation. Other workers have generally found that only small changes to empirical parameter values are needed upon moving from classical to path integral simulation methods. Since current AMOEBA parameters for other molecules also account for QNE implicitly,[50,51] we do the same here to maintain compatibility. In addition, explicit PIMD or RPMD calculations are significantly slower than classical molecular dynamics, and are often too compute intensive for large-scale biomolecular simulation. This implicit QNE protocol could reduce the transferability of AMOEBA, since cluster data on the quantum BO-PES is combined during parametrization with empirical classical MD accounting for QNE in only an average way. While the MD data used in fitting spans ambient and physiological temperatures, AMOEBA should provide a useful fit across that range.

A limitation common to most current empirical water potentials is their inability to explicitly treat proton dissociation. While potentials explicitly allowing proton dissociation were proposed over 35 years ago,[103] such models are not commonly used in molecular simulation.[104,105] More recently, several groups[106−108] have introduced a new generation of dissociable water models. Since a main intended use of the AMOEBA potential is for large-scale biomolecular and materials simulation, addition of proton dissociation capability would enable new approaches to modeling of pH-dependent systems.[109] This is an area we plan to address in a future extension of the AMOEBA model.

In summary, we have proposed a revised, effective AMOEBA potential for water. Considering the improved performance of the revised AMOEBA water model in bulk phase property prediction, we recommend implementation of these updated parameters for future studies employing the AMOEBA polarizable water model. While empirical, the model provides good estimates for a wide range of properties, and is reasonably transferable between the gas phase and the bulk phase, as well as in homogeneous and heterogeneous systems.

■ ASSOCIATED CONTENT

Supporting Information

This document contains tables with the experimental, AMOEBA14, and AMOEBA03 values and error bars for gas phase and bulk properties over the temperature range from 249 to 373 K. It also contains figures with calculated and experimental O−H and H−H radial distribution functions for liquid water at 298 K. This material is available free of charge via the Internet at http://pubs.acs.org.

■ AUTHOR INFORMATION

Corresponding Author

*Phone: (314) 935-4275. E-mail: ponder@dasher.wustl.edu.

Author Contributions

[‖]These authors contributed equally to this work.

Notes

The authors declare no competing financial interest.

■ ACKNOWLEDGMENTS

We would like to thank Branka Ladanyi for her many insightful scientific accomplishments in the field of dynamics and intermolecular structure in liquids. M.L.L. was supported in part by a Keck Fellowship from the Washington University School of Medicine and by NIH grant R01 GM106974. T.H.-G. is supported by NSF award CHE1265731. J.W.P. acknowledges support of the AMOEBA force field and the TINKER software that implements it by NSF award CHE1152823 and by NIH grant R01 GM106137. L.-P.W. and V.S.P. were supported by the Simbios National Center for Biocomputation (NIH Grant U54 GM072970).

■ REFERENCES

(1) Bernal, J. D.; Fowler, R. H. A Theory of Water and Ionic Solution, with Particular Reference to Hydrogen and Hydroxyl Ions. *J. Chem. Phys.* **1933**, *1*, 515−548.

(2) Jorgensen, W. L.; Chandrasekhar, J.; Madura, J. D.; Impey, R. W.; Klein, M. L. Comparison of Simple Potential Functions for Simulating Liquid Water. *J. Chem. Phys.* **1983**, *79*, 926−935.

(3) Rahman, A.; Stillinger, F. H. Molecular Dynamics Study of Liquid Water. *J. Chem. Phys.* **1971**, *55*, 3336−3359.

(4) Stillinger, F. H.; Rahman, A. Improved Simulation of Liquid Water by Moleculer Dynamics. *J. Chem. Phys.* **1974**, *60*, 1545−1557.

DOI: 10.1021/jp510896n
J. Phys. Chem. B 2015, 119, 9423−9437

(5) Berendsen, H. J. C.; Postma, J. P. M.; van Gunsteren, W. F.; Hermans, J. Interaction Models for Water in Relation to Protein Hydration. In *Intermolecular Forces*; Pullman, B., Ed.; Reidel: Dordrecht, The Netherlands, 1981; pp 331−342.
(6) Head-Gordon, T.; Stillinger, F. H. An Orientational Perturbation Theory for Pure Liquid Water. *J. Chem. Phys.* **1992**, *98*, 3313−3327.
(7) Mahoney, M. W.; Jorgensen, W. L. A Five-Site Model for Liquid Water and the Reproduction of the Density Anomoly by Rigid, Nonpolarizable Potential Functions. *J. Chem. Phys.* **2000**, *112*, 8910−8922.
(8) Berendsen, H. J. C.; Grigera, J. R.; Straatsma, T. P. The Missing Term in Effective Pair Potentials. *J. Phys. Chem.* **1987**, *91*, 6269−6271.
(9) Horn, H. W.; Swope, W. C.; Pitera, J. W.; Madura, J. D.; Dick, T. J.; Hura, G. L.; Head-Gordon, T. Development of an Improved Four-Site Water Model for Biomolecular Simulations: TIP4P-Ew. *J. Chem. Phys.* **2004**, *120*, 9665−9678.
(10) Levitt, M.; Hirshberg, M.; Sharon, R.; Laidig, K. E.; Daggett, V. Claibration and Testing of a Water Model for Simulation of the Molecular Dynamics of Proteins and Nucleic Acids in Solution. *J. Phys. Chem. B* **1997**, *101*, 5051−5061.
(11) Matsuoka, O.; Clementi, E.; Yoshimine, M. CI Study of the Water Dimer Potential Surface. *J. Chem. Phys.* **1976**, *64*, 1351−1361.
(12) Vesely, F. J. N-Particle Dynamics of Polarizable Stockmayer-type Molecules. *J. Comput. Phys.* **1977**, *24*, 361−371.
(13) Barnes, P.; Finney, J. L.; Nicholas, J. D.; Quinn, J. E. Cooperative Effects in Simulated Water. *Nature* **1979**, *282*, 459−464.
(14) Warshel, A.; Kuwajima, S. Incorporating Electric Polarizabilities in Water-Water Interaction Potentials. *J. Phys. Chem.* **1990**, *94*, 460−466.
(15) Sprik, M.; Klein, M. L. A Polarizable Model for Water Using Distributed Charge Sites. *J. Chem. Phys.* **1988**, *89*, 7556−7560.
(16) Wallqvist, A.; Ahlstrom, P.; Karlstrom, G. A New Intermolecular Energy Calculation Scheme: Applications to Potential Surface and Liquid Properties of Water. *J. Phys. Chem.* **1990**, *94*, 1649−1656.
(17) Caldwell, J.; Dang, L. X.; Kollman, P. A. Implementation of Nonadditive Intermolecular Potentials by Use of Molecular Dynamics: Development of a Water-Water Potential and Water-Ion Cluster Interactions. *J. Am. Chem. Soc.* **1990**, *112*, 9144−9147.
(18) Dykstra, C. E. Structures and Vibrational Frequencies of Small Water Complexes from Electrical Molecular Mechanics. *J. Chem. Phys.* **1989**, *91*, 6472−6476.
(19) Fanourgakis, G. S.; Xantheas, S. S. Development of Transferable Interaction Potentials for Water: V. Extension of the Flexible, Polarizable, Thole-Type Model Potential (TTM3-F, v.3.0) to Describe the Vibrational Spectra of Water Clusters and Liquid Water. *J. Chem. Phys.* **2008**, *128*, 154519.
(20) Lamoureux, G.; Harder, E.; Vorobyov, I. V.; Roux, B.; MacKerell, A. D. A Polarizable Model of Water for Molecular Dynamics Simulations of Biomolecules. *Chem. Phys. Lett.* **2006**, *418*, 245−249.
(21) Kumar, R.; Wang, F. F.; Jenness, G. R.; Jordan, K. D. A Second Generation Distributed Point Polarizable Water Model. *J. Chem. Phys.* **2010**, *132*, 014309.
(22) Williams, D. E. Representation of the Molecular Electrostatic Potential by Atomic Multipole and Bond Dipole Models. *J. Comput. Chem.* **1988**, *9*, 745−763.
(23) Bayly, C. I.; Cieplak, P.; Cornell, W. D.; Kollman, P. A. A Well-Behaved Electrostatic Potential Based Method Using Charge Restraints for Deriving Atomic Charges: The RESP Model. *J. Phys. Chem.* **1993**, *97*, 10269−10280.
(24) Mao, A. H.; Pappu, R. V. Crystal Lattice Properties Fully Determine Short-Range Interaction Parameters for Alkali and Halide Ions. *J. Chem. Phys.* **2012**, *137*, 064104.
(25) Grossfield, A.; Ren, P. Y.; Ponder, J. W. Ion Solvation Thermodynamics from Simulation with a Polarizable Force Field. *J. Am. Chem. Soc.* **2003**, *125*, 15671−15682.
(26) Berne, B. J.; Thirumalai, D. On the Simulation of Quantum Systems: Path Integral Methods. *Annu. Rev. Phys. Chem.* **1986**, *37*, 401−424.
(27) Habershon, S.; Manolopoulos, D. E.; Markland, T. E.; Miller, T. F. I. Ring-Polymer Molecular Dynamics: Quantum Effects in Chemical Dynamics from Classical Trajectories in an Extended Phase Space. *Annu. Rev. Phys. Chem.* **2013**, *64*, 387−413.
(28) Kuharski, R. A.; Rossky, P. J. Quantum Mechanical Contributions to the Structure of Liquid Water. *Chem. Phys. Lett.* **1984**, *103*, 357−362.
(29) Billeter, S. R.; King, P. M.; van Gunsteren, W. F. Can the Density Maximum of Water by found by Computer Simulation? *J. Chem. Phys.* **1994**, *100*, 6692−6699.
(30) Lobaugh, J.; Voth, G. A. A Quantum Model for Water: Equilibrium and Dynamical Properties. *J. Chem. Phys.* **1997**, *106*, 2400−2410.
(31) Guillot, B.; Guissani, Y. Quantum Effects in Simulated Water by the Feynman-Hibbs Approach. *J. Chem. Phys.* **1998**, *108*, 10162−10174.
(32) Mahoney, M. W.; Jorgensen, W. L. Quantum, Intramolecular Flexibility, and Polarizability Effects on the Reproduction of the Density Anomaly of Liquid Water by Simple Potential Functions. *J. Chem. Phys.* **2001**, *115*, 10758−10768.
(33) Stern, H. A.; Berne, B. J. Quantum Effects in Liquid Water: Path-Integral Simulations of a Flexible and Polarizable ab Initio Model. *J. Chem. Phys.* **2001**, *115*, 7622−7628.
(34) Paesani, F.; Zhang, W.; Case, D. A.; Cheatham, T. E. I.; Voth, G. A. An Accurate and Simple Quantum Model for Liquid Water. *J. Chem. Phys.* **2006**, *125*, 184507.
(35) Habershon, S.; Markland, T. E.; Manolopoulos, D. E. Competing Quantum Effects in the Dynamics of a Flexible Water Model. *J. Chem. Phys.* **2009**, *131*, 024501.
(36) Markland, T. E.; Berne, B. J. Unraveling Quantum Mechanical Effects in Water Using Isotopic Fractionation. *Proc. Natl. Acad. Sci. U.S.A.* **2012**, *109*, 7988−7991.
(37) Berens, P. H.; H, M. D.; White, G. M.; Wilson, K. R. Thermodynamics and Quantum Corrections from Molecular Dynamics for Liquid Water. *J. Chem. Phys.* **1983**, *79*, 2375−2389.
(38) Cerutti, D. S.; Swope, W. C.; Rice, J. E.; Case, D. A. ff14ipq: A Self-Consistent Force Field for Condensed-Phase Simulations of Proteins. *J. Chem. Theory Comput.* **2014**, *10*, 4515−4534.
(39) Nerenberg, P. S.; Jo, B.; So, C.; Tripathy, A.; Head-Gordon, T. Optimizing Solute-Water van der Waals Interactions to Reproduce Solvation Rree Energies. *J. Phys. Chem. B* **2012**, *116*, 4524−4534.
(40) Lifson, S.; Warshel, A. Consistent Force Field for Calculations of Conformations, Vibrational Spectra, and Enthalpies of Cycloalkane and n-Alkane Molecules. *J. Chem. Phys.* **1968**, *49*, 5116−5129.
(41) Maple, J. R.; Hwang, M. J.; Stockfisch, T. P.; Dinur, U.; Waldman, M.; Ewig, C. S.; Hagler, A. T. Derivation of Class-II Force Fields. 1. Methodology and Quantum Force Field for the Alkyl Functional Group and Alkane Molecules. *J. Comput. Chem.* **1994**, *15*, 162−182.
(42) Williams, D. E. Transferable Empirical Nonbonded Potential Functions. *Top. Curr. Phys.* **1981**, *26*, 3−40.
(43) Ercolessi, F.; Adams, J. B. Interatomic Potentials from 1st-Principles Calculations- The Force-Matching Method. *Europhys. Lett.* **1994**, *26*, 583−588.
(44) Izvekov, S.; Parrinello, M.; Burnham, C. J.; Voth, G. A. Effective Force Fields for Condensed Phase Systems from ab Initio Molecular Dynamics Simulation: A New Method for Force-Matching. *J. Chem. Phys.* **2004**, *120*, 10896−10913.
(45) Akin-Ojo, O.; Song, Y.; Wang, F. Developing ab Initio Quality Force Fields from Condensed Phase Quantum-Mechanics/Molecular-Mechanics Calculations through the Adaptive Force Matching Method. *J. Chem. Phys.* **2008**, *129*, 064108.
(46) Wang, L.-P. *ForceBalance: Systematic Force Field Optimization*, https://simtk.org/home/forcebalance/, Stanford University, March 2014.
(47) Wang, L.-P.; Chen, J.; van Voorhis, T. Systematic Parametrization of Polarizable Force Fields from Quantum Chemistry Data. *J. Chem. Theory Comput.* **2013**, *9*, 452−460.
(48) Wang, L.-P.; Martinez, T. J.; Pande, V. S. Building Force Fields - An Automatic, Systematic, and Reproducible Approach. *J. Phys. Chem. Lett.* **2014**, *5*, 1885−1891.
(49) Ren, P. Y.; Ponder, J. W. Polarizable Atomic Multipole Water Model for Molecular Mechanics Simulation. *J. Phys. Chem. B* **2003**, *107*, 5933−5947.

DOI: 10.1021/jp510896n
J. Phys. Chem. B 2015, 119, 9423−9437

(50) Ren, P.; Wu, C.; Ponder, J. W. Polarizable Atomic Multipole-based Molecular Mechanics for Organic Molecules. *J. Chem. Theory Comput.* **2011**, *7*, 3143−3161.
(51) Shi, Y.; Xia, Z.; Zhang, J.; Best, R.; Wu, C.; Ponder, J. W.; Ren, P. The Polarizable Atomic Multipole-based AMOEBA Force Field for Proteins. *J. Chem. Theory Comput.* **2013**, *9*, 4046−4063.
(52) Halgren, T. A. The Representation of van der Waals (vdW) Interactions in Molecular Mechanics Force Fields: Potential Form, Combination Rules, and vdW Parameters. *J. Am. Chem. Soc.* **1992**, *114*, 7827−7843.
(53) Thole, B. T. Molecular Polarizabilities Calculated with a Modified Dipole Interaction. *Chem. Phys.* **1981**, *59*, 341−350.
(54) Martyna, G. J.; Tuckerman, M. E.; Tobias, D. J.; Klein, M. L. Explicit Reversible Integrators for Extended Systems Dynamics. *Mol. Phys.* **1996**, *87*, 1117−1157.
(55) Ponder, J. W. *TINKER: Software Tools for Molecular Design*, version 7.0, http://dasher.wustl.edu/tinker/, Washington University in St. Louis, June 2014.
(56) Eastman, P.; Friedrichs, M. S.; Chodera, J. D.; Radmer, R. J.; Bruns, C. M.; Ku, J. P.; Beauchamp, K. A.; Lane, T. J.; Wang, L.-P.; Shukla, D.; et al. OpenMM 4: A Reusable, Extensible, Hardware Independent Library for High Performance Molecular Simulation. *J. Chem. Theory Comput.* **2013**, *9*, 461−469.
(57) Smith, B. J.; Swanton, D. J.; Pople, J. A.; Schaefer, H. F.; Radom, L. Transition Structures for the Interchange of Hydrogen Atoms within the Water Dimer. *J. Chem. Phys.* **1990**, *92*, 1240−1247.
(58) Bates, D. M.; Tschumper, G. S. CCSD(T) Complete Basis Set Limit Relative Energies for Low-Lying Water Hexamer Structures. *J. Phys. Chem. A* **2009**, *113* (15), 3555−3559.
(59) Xantheas, S. S.; Apra, E. The Binding Energies of the D2d and S4 Water Octamer Isomers: High-Level Electronic Structure and Empirical Potential Results. *J. Chem. Phys.* **2004**, *120*, 823−828.
(60) Bulusu, S.; Yoo, S.; Apra, E.; Xantheas, S.; Zeng, X. C. Lowest-Energy Structures of Water Clusters (H2O)11 and (H2O)13. *J. Phys. Chem. A* **2006**, *110* (42), 11781−11784.
(61) Fanourgakis, G. S.; Apra, E.; Xantheas, S. S. High-level ab Initio Calculations for the Four Low-Lying Families of Minima of (H2O)20. I. Estimates of MP2/CBS Binding Energies and Comparison with Empirical Potentials. *J. Chem. Phys.* **2004**, *121*, 2655−2663.
(62) Fanourgakis, G. S.; Apra, E.; de Jong, W. A.; Xantheas, S. S. High-Level ab Initio Calculations for the Four Low-Lying Families of Minima of (H2O)20. II. Spectroscopic Signatures of the Dodecahedron, Fused Cubes, Face-Sharing Pentagonal Prisms, and Edge-Sharing Pentagonal Prisms Hydrogen Bonding Networks. *J. Chem. Phys.* **2005**, *122*, 134304.
(63) Wang, L. P.; Head-Gordon, T.; Ponder, J. W.; Ren, P.; Chodera, J. D.; Eastman, P. K.; Martinez, T. J.; Pande, V. S. Systematic Improvement of a Classical Molecular Model of Water. *J. Phys. Chem. B* **2013**, *117*, 9956−9972.
(64) Steele, R. P.; DiStasio, R. A., Jr.; Shao, Y.; Kong, J.; Head-Gordon, M. Dual-Basis Second-Order M?ller-Plesset Perturbation Theory: A Reduced-Cost Reference for Correlation Calculations. *J. Chem. Phys.* **2006**, *125*, 074108.
(65) Steele, R. P.; DiStasio, R. A.; Head-Gordon, M. Non-Covalent Interactions with Dual-Basis Methods: Pairings for Augmented Basis Sets. *J. Chem. Theory Comput.* **2009**, *5*, 1560−1572.
(66) Dunning, T. H. Gaussian Basis Sets for Use in Correlated Molecular Calculations. I. The Atoms Boron through Neon and Hydrogen. *J. Chem. Phys.* **1989**, *90*, 1007−1023.
(67) Shao, Y.; Molnar, L. F.; Jung, Y.; Kussmann, J.; Ochsenfeld, C.; Brown, S. T.; Gilbert, A. T.; Slipchenko, L. V.; Levchenko, S. V.; O'Neill, D. P.; et al. Advances in Methods and Algorithms in a Modern Quantum Chemistry Program Package. *Phys. Chem. Chem. Phys.* **2006**, *8*, 3172−3191.
(68) Ren, P. Y.; Ponder, J. W. Temperature and Pressure Dependence of the AMOEBA Water Model. *J. Phys. Chem. B* **2004**, *108*, 13427−13437.
(69) Levenberg, K. A Method for the Solution of Certain Non-Linear Problems in Least Squares. *Q. Appl. Math.* **1944**, *2*, 164−168.
(70) Marquardt, D. W. An Algorithm for Least-Squares Estimation of Nonlinear Parameters. *J. Soc. Ind. Appl. Math.* **1963**, *11*, 431−441.
(71) Dennis, J. E.; Gay, D. M.; Welsch, R. E. An Adaptive Non-Linear Least-Squares Algorithm. *ACM Trans. Math. Software* **1981**, *7*, 348−368.
(72) More, J. J.; Sorensen, D. C. Computing a Trust Region. *SIAM J. Sci. Stat. Comp.* **1983**, *4*, 553−572.
(73) Di Pierro, M.; Elber, R. Automated Optimization of Potential Parameters. *J. Chem. Theory Comput.* **2013**, *9*, 3311−3320.
(74) Bui, P.; Rajan, D.; Abdul-Wahid, B.; Izaguirre, J. A.; Thain, D. In *Work Queue + Python: A Framework For Scalable Scientific Ensemble Applications*; Workshop on Python for High Performance and Scientific Computing (PyHPC): Seattle, WA, 2011.
(75) Shirts, M. R.; Chodera, J. D. Statistically Optimal Analysis of Samples from Multiple Equilibrium States. *J. Chem. Phys.* **2008**, *129*, 124105.
(76) Millot, C.; Soetens, J.-C.; Martins Costa, M. T. C.; Hodges, M. P.; Stone, A. J. Revised Anisotropic Site Potentials for the Water Dimer and Calculated Properties. *J. Phys. Chem. A* **1998**, *102*, 754−770.
(77) Benjamin, K. M.; Schultz, A. J.; Kofke, D. A. Virial Coefficients of Polarizable Water Applications to Thermodynamic Properties and Molecular Clustering. *J. Phys. Chem. C* **2007**, *111*, 16021−16027.
(78) Bustos Marun, R. A.; Coronado, E. A.; Ferrero, J. C. Second Virial Coefficients of Water Beyond the Conventional First-Order Quantum Correction. *Chem. Phys. Lett.* **2005**, *405*, 203−207.
(79) Nymand, T. M.; Astrand, P. O. Calculation of the Geometry of the Water Molecule in Liquid Water. *J. Phys. Chem. A* **1997**, *101*, 10039−10044.
(80) Ichikawa, K.; Kameda, Y.; Yamaguchi, T.; Wakita, H.; Misawa, M. Neutron-Diffraction Investigation of the Intramolecular Structure of a Water Molecule in the Liquid-Phase at High-Temperatures. *Mol. Phys.* **1991**, *73*, 79−86.
(81) Debenedetti, P. G.; Stanley, H. E. Supercooled and Glassy Water. *Phys. Today* **2003**, No. June, 40−46.
(82) Carnie, S. L.; Patey, G. N. Fluids of Polarizable Hard-Spheres with Dipoles and Tetrahedral Quadrupoles- Integral-Equation Results with Application to Liquid Water. *Mol. Phys.* **1982**, *47*, 1129−1151.
(83) Head-Gordon, T.; Rick, S. W. Consequences of Chain Networks on Thermodynamic, Dielectric and Structural Properties for Liquid Water. *Phys. Chem. Chem. Phys.* **2007**, *9*, 83−91.
(84) Soper, A. K.; Phillips, M. G. A New Determination of the Structure of Water at 25-Degrees-C. *Chem. Phys.* **1986**, *107*, 47−60.
(85) Soper, A. K. The Radial Distribution Functions of Water and Ice from 220 to 673 K and at Pressures up to 400 MPa. *Chem. Phys.* **2000**, *258*, 121−137.
(86) Sorenson, J. M.; Hura, G.; Glaeser, R. M.; Head-Gordon, T. What Can X-ray Scattering Tell Us about the Radial Distribution Functions of Water? *J. Chem. Phys.* **2000**, *113*, 9149−9161.
(87) Skinner, L. B.; Huang, C.; Schlesinger, D.; Pettersson, L. G.; Nilsson, A.; Benmore, C. J. Benchmark Oxygen-Oxygen Pair-Distribution Function of Ambient Water from X-ray Diffraction Measurements with a Wide Q-Range. *J. Chem. Phys.* **2013**, *138*, 074506.
(88) Hura, G.; Sorenson, J. M.; Glaeser, R. M.; Head-Gordon, T. A High-Quality X-Ray Scattering Experiment on Liquid Water at Ambient Conditions. *J. Chem. Phys.* **2000**, *113*, 9140−9148.
(89) Morita, A. Water Polarizability in Condensed Phase: Ab Initio Evaluation by Cluster Approach. *J. Comput. Chem.* **2002**, *23*, 1466−1471.
(90) Salanne, M.; Vuilleumier, R.; Madden, P. A.; Simon, C.; Turq, P.; Guillot, B. Polarizabilities of Individual Molecules and Ions in Liquids from First Principles. *J. Phys.: Condens. Matter* **2008**, *20*, 494207.
(91) Harris, K. R.; Woolf, L. A. Temperature and Volume Dependence of the Viscosity of Water and Heavy Water at Low Temperature. *J. Chem. Phys. Ref. Data* **2004**, *49*, 1064−1069.
(92) Yeh, I.-C.; Hummer, G. System-Size Dependence of Diffusion Coefficients and Viscosities from Molecular Dynamics Simulations with Periodic Boundary Conditions. *J. Phys. Chem. B* **2004**, *108*, 15873−15879.

DOI: 10.1021/jp510896n
J. Phys. Chem. B 2015, 119, 9423−9437

(93) IAPWS Release on the Surface Tension of Ordinary Water Substance, *International Association for the Properties of Water and Steam*, September 1994, London, England.
(94) Zheng, L.; Chen, M.; Yang, W. Random Walk in Orthogonal Space to Achieve Efficient Free-Energy Simulation of Complex Systems. *Proc. Natl. Acad. Sci. U.S.A.* **2008**, *105*, 20227−20232.
(95) Palmo, K.; Mannfors, B.; Mirkin, N. G.; Krimm, S. Inclusion of Charge and Polarizability Fluxes Provides Needed Physical Accuracy in Molecular Mechanics Force Fields. *Chem. Phys. Lett.* **2006**, *429*, 628−632.
(96) Fanourgakis, G. S.; Xantheas, S. S. The Bend Angle of Water in Iced Ih and Liquid Water: The Significance of Implementing the Nonlinear Monomer Dipole Moment Surface in Classical Interaction Potentials. *J. Chem. Phys.* **2006**, *124*, 174504.
(97) Guillot, B.; Guissani, Y. How to Build a Better Pair Potential for Water. *J. Chem. Phys.* **2001**, *114*, 6720−6733.
(98) Piquemal, J.-P.; Gresh, N.; Giessner-Prettre, C. Improved Formulas for the Calculation of the Electrostatic Contribution to the Intermolecular Interaction Energy from Multipolar Expansion of the Electronic Distribution. *J. Phys. Chem. A* **2003**, *107*, 10353−10359.
(99) Wang, B.; Truhlar, D. G. Screened Electrostatic Interactions in Molecular Mechanics. *J. Chem. Theory Comput.* **2014**, *10*, 4480−4487.
(100) Tafipolsky, M.; Engels, B. Accurate Intermolecular Potentials with Physically Grounded Electrostatics. *J. Chem. Theory Comput.* **2011**, *7*, 1791−1803.
(101) Freitag, M. A.; Gordon, M. S.; Jansen, J. H.; Stevens, W. J. Evaluation of Charge Penetration between Distributed Multipolar Expansions. *J. Chem. Phys.* **2000**, *112*, 7300−7306.
(102) Slipchenko, L. V.; Gordon, M. S. Electrostatic Energy in the Effective Fragment Potential Method: Theory and Application to Benzene Dimer. *J. Comput. Chem.* **2006**, *28*, 276−291.
(103) Stillinger, F. H.; Carl, C. W. Polarization Model for Water and its Ionic Dissociation Products. *J. Chem. Phys.* **1978**, *69*, 1473−1484.
(104) Halley, J. W.; Rustad, J. R.; Rahman, A. A Polarizable, Dissociating Molecular Dynamics Model for Liquid Water. *J. Chem. Phys.* **1993**, *98*, 4110−4119.
(105) Carl, C. W. A Variable Charge Central Force Model of Water and its Ionic Dissociation Products. *J. Chem. Phys.* **1996**, *104*, 7255−7260.
(106) Lussetti, E.; Pastore, G.; Smargiassi, E. A Fully Polarizable and Dissociable Potential for Water. *Chem. Phys. Lett.* **2003**, *381*, 287−291.
(107) Kale, S.; Herzfeld, J.; Dai, S.; Blank, M. Lewis-Inspired Representation of Dissociable Water in Clusters and Grotthuss Chains. *J. Biol. Phys.* **2012**, *38*, 49−59.
(108) Pinilla, C.; Irani, A. H.; Seriani, N.; Scandolo, S. Ab Initio Parameterization of an All-Atom Polarizable and Dissociable Force Field for Water. *J. Chem. Phys.* **2012**, *135*, 114511.
(109) Chen, W.; Morrow, B. H.; Shi, C.; Shen, J. K. Recent Development and Application of Constant pH Molecular Dynamics. *Mol. Simul.* **2014**, *40*, 830−838.
(110) Clough, S. A.; Beers, Y.; Klein, G. P.; Rothman, L. S. Dipole-Moment of Water from Stark Measurements of H2O, HDO, and D2O. *J. Chem. Phys.* **1973**, *59*, 2254−2259.
(111) Verhoeven, J.; Dymanus, A. Magnetic Properties and Molecular Quadrupole Tensor of the Water Molecule by Beam-Maser Zeeman Spectroscopy. *J. Chem. Phys.* **1970**, *52*, 3222−3233.
(112) Murphy, W. F. The Rayleigh Depolarization Ratio and Rotational Raman Spectrum of Water Vapor and the Polarizability Components for the Water Molecule. *J. Chem. Phys.* **1977**, *67*, 5877−5882.
(113) Curtiss, L. A.; Frurip, D. J.; Blander, M. Studies of Molecular Association in H2O and D2O Vapors by Measurement of Thermal Conductivity. *J. Chem. Phys.* **1979**, *71*, 2703−2711.
(114) Odutola, J. A.; Dyke, T. R. Partially Deuterated Water Dimers - Microwave-Spectra and Structure. *J. Chem. Phys.* **1980**, *72*, 5062−5070.
(115) Tschumper, G. S.; Leininger, M. L.; Hoffman, B. C.; Valeev, E. F.; Schaefer, H. F.; Quack, M. Anchoring the Water Dimer Potential Energy Surface with Explicitly Correlated Computations and Focal Point Analyses. *J. Chem. Phys.* **2002**, *116*, 690−701.
(116) Klopper, W.; van Duijneveldt-van de Rijdt, J. G. C. M.; van Duijneveldt, F. B. Computational Determination of Equilibrium Geometry and Dissociation Energy of the Water Dimer. *Phys. Chem. Chem. Phys.* **2000**, *2*, 2227−2234.
(117) Lee, H. M.; Suh, S. B.; Lee, J. Y.; Tarakeshwar, P.; Kim, K. S. Structures, Energies, Vibrational Spectra, and Electronic Properties of Water Monomer to Decamer. *J. Chem. Phys.* **2000**, *112*, 9759−9772.
(118) van Duijneveldt-van de Rijdt, J. G. C. M.; Mooij, W. T. M.; van Duijneveldt, F. B. Testing the Quality of Some Recent Water−Water Potentials. *Phys. Chem. Chem. Phys.* **2003**, *5*, 1169−1180.
(119) Yoo, S.; Aprà, E.; Zeng, X. C.; Xantheas, S. S. High-Level Ab Initio Electronic Structure Calculations of Water Clusters (H2O)16 and (H2O)17: A New Global Minimum for (H2O)16. *J. Phys. Chem. Lett.* **2010**, *1*, 3122−3127.
(120) Wagner, W.; Pruss, A. The IAPWS Formulation 1995 for the Thermodynamic Properties of Ordinary Water Substance for General and Scientific Use. *J. Phys. Chem. Ref. Data* **2002**, *31*, 387−535.
(121) Schmid, R.; Miah, A. M.; Sapunov, V. N. A New Table of the Thermodynamic Quantities of Ionic Hydration: Values and Some Applications. *Phys. Chem. Chem. Phys.* **2000**, *2*, 97−102.
(122) Feller, D.; Glendening, E. D.; Woon, D. E.; Feyereisen, M. W. An Extended Basis-Set Ab-Initio Study of Alkali-Metal Cation-Water Clusters. *J. Chem. Phys.* **1995**, *103*, 3526−3542.
(123) Xantheas, S. S. Quantitative Description of Hydrogen Bonding in Chloride-Water Clusters. *J. Phys. Chem.* **1996**, *100*, 9703−9713.
(124) Lide, D. R. *CRC Handbook of Chemistry and Physics*, 82nd ed.; CRC Press LLC: Boca Raton, FL, 2001.
(125) Kell, G. S.; McLaurin, G. E.; Whalley, E. PVT Properties of Water VII. Vapour Densities of Light and Heavy Water from 150 to 500 C. *Proc. R. Soc. A* **1989**, *425*, 49−71.
(126) Kell, G. S. Density, Thermal Expansivity, and Compressibility of Liquid Water from 0 deg. to 150 deg. Correlations and Tables for Atmospheric Pressure and Saturation Reviewed and Expressed on 1968 Temperature Scale. *J. Chem. Phys. Ref. Data* **1975**, *20*, 97−105.

NOTE ADDED AFTER ASAP PUBLICATION

This paper was published ASAP on February 26, 2015, with incorrect data in the iAMOEBA column of Table 6. The corrected version was reposted on March 3, 2015.

DOI: 10.1021/jp510896n
J. Phys. Chem. B 2015, 119, 9423−9437